

37 *Abstract*—Precipitation is a key source of freshwater; therefore observing global patterns of
38 precipitation and its intensity is important for science, society, and understanding our planet in a
39 changing climate. In 2014, NASA and the Japan Aerospace Exploration Agency (JAXA)
40 launched the Global Precipitation Measurement (GPM) Core Observatory (GPM-CO) spacecraft.
41 The GPM-CO carries the most advanced precipitation sensors currently in space including a
42 dual-frequency precipitation radar provided by JAXA measuring the three-dimensional
43 structures of precipitation and a well-calibrated, multi-frequency passive microwave radiometer
44 providing wide-swath precipitation data. The GPM-CO was designed to measure rain rates from
45 0.2-110.0 mm h⁻¹ and to detect moderate to intense snow events. The GPM-CO serves as a
46 reference for unifying the data from a constellation of partner satellites to provide next-
47 generation, merged precipitation estimates globally and with high spatial and temporal
48 resolutions. Through improved measurements of rain and snow, precipitation data from GPM
49 provides new information such as: details on precipitation structure and intensity; observations of
50 hurricanes and typhoons as they transition from the tropics to mid-latitudes; data to advance
51 near-real-time hazard assessment for floods, landslides and droughts; inputs to improve weather
52 and climate models; and insights into agricultural productivity, famine, and public health. Since
53 launch, GPM teams have calibrated satellite instruments, refined precipitation retrieval
54 algorithms, expanded science investigations, and processed and disseminated precipitation data
55 for a range of applications. The current status of GPM, its ongoing science, and future plans will
56 be presented.

57 **Introduction and Motivation**

58 Water is essential to our planet, Earth. It literally moves mountains through erosion; transports
59 heat in Earth's oceans and atmosphere; keeps our planet from freezing due to radiative impacts of
60 atmospheric water vapor; causes catastrophes through droughts, floods, landslides, blizzards, and
61 severe storms; but most importantly water is vital for nourishing all life on Earth. Precipitation as
62 a source of freshwater links the Earth's water and energy cycles. Thus knowing when, where, and
63 how precipitation falls is of paramount importance for science and society.

64 While there are areas of the world that have dense ground-based sensors for measuring
65 precipitation in the form of rain gauges and radars, the vast oceans, less populated regions, and
66 parts of developing countries lack adequate surface measurements of precipitation (Kidd et al.
67 2016). Satellites provide an optimal platform from which to measure precipitation globally. In
68 1997, NASA and the National Space Development Agency of Japan (NASDA), now the Japan
69 Aerospace Exploration Agency (JAXA), launched the Tropical Rainfall Measuring Mission
70 (TRMM) (Simpson et al. 1998, Kummerow et al. 1998, 2000), which operated until April 2015.
71 The TRMM spacecraft had both a passive microwave multi-frequency imaging radiometer
72 (provided by NASA) and a Ku-band radar channel (provided by NASDA) capable of generating
73 three-dimensional views of precipitation structure (Kozu et al. 2001). TRMM's data continue to
74 foster important scientific investigations such as Curtis et al. (2007), Adler et al. (2009), Shepherd
75 et al. (2011), Liu et al. (2012), Houze et al. (2015), and Liu and Zipser (2015). In addition, TRMM
76 has a large user community that has applied these data operationally to support decision making
77 (Kirschbaum et al., 2016).

78 The Global Precipitation Measurement (GPM) Core Observatory (GPM-CO) spacecraft is an
79 advanced successor to TRMM, with additional channels on both the Dual-frequency Precipitation
80 Radar (DPR) and on the GPM Microwave Imager (GMI) with capabilities to sense light rain and
81 falling snow (Hou et al. 2014, Hou et al. 2008). The GPM-CO, also a NASA-JAXA partnership,
82 was launched in February 2014 and currently operates in a non-sun-synchronous orbit with an
83 inclination angle of 65°. This orbit allows the GPM-CO to sample precipitation across all hours of
84 the day from the tropics to the Arctic and Antarctic circles and for observing hurricanes and
85 typhoons as they transition from the tropics to mid-latitudes. GPM expands TRMM's reach not
86 only in terms of global coverage, but also through sophisticated satellite instrumentation, the inter-
87 calibration of datasets from other microwave radiometers, coordinated merged precipitation data
88 sets, reduced latency for delivering data products, simplified data access, expanded global ground
89 validation efforts, and integrated user applications. Because of the application focus of GPM, the
90 public release of precipitation products is required in near-real-time (1-5 hours after the
91 observations are downlinked to the ground stations).

92 The GPM mission has several scientific objectives including (1) advancing precipitation
93 measurements from space, (2) improving knowledge of precipitation systems, water cycle
94 variability and freshwater availability, (3) improving climate modeling and prediction, (4)
95 improving weather forecasting and four-dimensional (4D) reanalysis, and (5) improving
96 hydrological modeling and prediction. More details about these scientific objectives can be found
97 in Hou et al. (2014).

98 The GPM-CO well-calibrated instruments allow for scientifically-advanced observations of
99 precipitation in the mid-latitudes where a majority of the Earth's population lives. The central

100 panel of Figure 1 shows the coverage of the GPM-CO, and several interesting precipitation events
101 are shown in panels a-l. These examples indicate the breadth of GPM's observational capabilities
102 through measurements of diverse weather systems, such as severe convection, falling snow, light
103 rain, and frontal systems over both land and ocean. The measurements include surface precipitation
104 rates available from GMI and 3-dimensional precipitation structure from DPR.

105 A founding concept of the GPM mission is the constellation of precipitation observations
106 provided by national and international satellite partners of opportunity. International and national
107 partnerships are formed independently by both NASA and JAXA for sharing satellite data, ground
108 validation measurements, and scientific expertise (Hou et al. 2014). The GPM-CO serves as a
109 calibrator to ensure unified precipitation estimates from all satellite partners at high temporal (0.5
110 to 3.0 hours) and spatial (5 to 15 km) scales (Hou et al. 2014). Such satellite precipitation datasets
111 can be merged via algorithms and accumulated over time as shown in Figure 2. These GPM products
112 allow for detailed investigations of how and where precipitation is distributed and how these
113 patterns change over days, seasons, and years. These estimates are also used to model and estimate
114 hazard impacts (e.g. floods and droughts), weather related disasters, agricultural forecasting, and
115 famine warnings (Kirschbaum et al., 2016).

116 The GPM-CO instruments and constellation concept will be discussed in Section 2.
117 Precipitation retrieval algorithms, data products, processing, and availability will be presented in
118 Section 3. Section 4 will be devoted to early validation results. In Section 5, the paper will
119 summarize how GPM data have been used over the past two years for selected scientific
120 investigations and societal applications. Material presented herein is primarily from the U.S.
121 Science Team. Nevertheless, it is important to note that the current and future successes of GPM

122 are joint with our international partners, especially Japan. The paper will close with conclusions
123 and next steps.

124

125 **GPM Core Observatory and Constellation Configuration**

126 An essential activity of the GPM mission is the use of the NASA-JAXA GPM-CO to unify
127 and inter-calibrate data sets generated by constellation satellite partners and merge these into next-
128 generation, high temporal resolution global precipitation estimates. Fundamental to the success of
129 this activity is both the GPM-CO instrumentation and the constellation configuration.

130

131 *GPM Core Observatory*

132 The GPM-CO was launched February 28, 2014 at 3:37am JST (February 27, 2014 18:37 UTC)
133 from Tanegashima Island, Japan. The prime mission lifetime (instrument design life) is 3 years
134 and 2 months (for checkout) but fuel is projected to last well beyond that, potentially lasting 15 or
135 more years if the instruments/spacecraft systems (e.g., batteries) do not fail and fuel requirements
136 do not increase. The GMI and DPR together provide a powerful synergistic tool to assess
137 precipitation micro- and macro-structure, intensity and phase globally at relatively high (regional)
138 resolutions. The DPR with Ku-band (35.5 GHz) and Ka-band (13.6 GHz) channels provides three-
139 dimensional (3D) precipitation (rain and snow) particle structure with vertical resolution of 250m,
140 a horizontal resolution of ~5 km, and swath width of 125 km (Ka) and 245 km (Ku) (Hou et al.
141 2014). The DPR was extensively calibrated pre-launch (Kojima et al., 2013) and its performance
142 meets mission requirements (e.g., Kubota et al. 2015, Kubota et al. 2016, Toyoshima et al. 2015).
143 (See also the sidebar on GPM's Mission Science Requirements.)

144 The GMI is a 13 channel conically scanning microwave radiometer (see Table 1 and Hou et al.
145 2014 for details). GMI provides wide-swath (885 km) TB data to estimate surface precipitation at
146 resolutions ranging from 5-25 km depending on frequency. Design requirements for GMI were
147 driven both by requirements to build *a priori* databases to support Bayesian microwave
148 precipitation retrieval algorithms (Kummerow et al. 2010, Kummerow et al. 2015) as well as to
149 provide a reference radiance calibration standard for the GPM constellation (Hou et al. 2014). The
150 design features needed to meet the requirements include a shroud over the warm load to eliminate
151 solar intrusions, a robust reflective antenna coating to minimize emissivity issues, and the addition
152 of noise diodes for a four point calibration of the window channels (Draper et al. 2013, 2015a,
153 2015b). The GMI instrument is meeting its performance requirements (Draper et al. 2015) and has
154 already been deemed one of the best calibrated conically scanning passive microwave radiometers
155 in space with brightness temperature accuracy for all channels within 0.4K and stability within
156 0.2K (Wentz and Draper, 2016).

157

158 *GPM Constellation Configuration*

159 The GPM mission encompasses the GPM-CO and a constellation of about 10 satellites (as of
160 mid-2016) from national and international partners of opportunity [see Table 1 and Hou et al. 2014
161 for details]. These satellites are designed and operated for the partners' missions, but these agencies
162 are willing to share their data with GPM for the purpose of producing next-generation unified
163 global precipitation estimates. The constellation satellites bearing passive radiometers fly
164 independent polar or non-sun-synchronous orbits allowing for multiple coincident overpasses with
165 the GPM-CO.

166 For the constellation partner data, the first step toward unified precipitation estimates is the
167 inter-calibration of brightness temperatures (TB) using GMI as the reference standard. This
168 ensures that the observed TB are consistent among the sensors with expected differences after
169 accounting for variations in the observing frequencies, bandwidths, polarizations, and view angles
170 (see Wilheit 2013, Wilheit et al. 2015, Zavadsky et al. 2013, Zhang et al. 2011, 2016 and Table 1).
171 Figure 3 shows the extent of coverage provided by single 98-minute orbits for each of the various
172 radiometer types in the GPM constellation.

173 Sensor inter-calibration between GMI and the partner sensors involves several steps, as
174 described in Wilheit (2013, 2015) and Berg et al. (2016). Multiple independent approaches are
175 compared during these steps, which help to identify flaws or limitations of a given approach, thus
176 increasing confidence in the results and providing a measure of the uncertainty in the resulting
177 calibration adjustments. After adjustments, residual differences between GMI channels and those
178 on the constellation radiometers are generally smaller than 1 K (Berg et al. 2016). This is a
179 remarkable achievement that now allows the project to focus on the precipitation products rather
180 than TB uncertainties.

181 Future satellite inter-calibration tasks include understanding and quantifying the residual
182 uncertainties in the estimated calibration differences due to the radiative transfer models and
183 geophysical parameter retrievals and adapting to changes in the radiometer constellation. Updates
184 in the GMI calibration algorithms and subsequent inter-calibration adjustments to the constellation
185 sensors will occur during scheduled reprocessing of retrieval products. In addition, inter-
186 calibrating TRMM's TMI and pre-GPM microwave constellation sensor data to GMI is necessary

187 for generating a consistent long-term next-generation precipitation record that covers the TRMM
188 and GPM eras.

189

190 **Algorithms, Data Products, Data Processing and Data Availability**

191 The GPM-CO data processing is a joint NASA/JAXA effort. NASA data processing is
192 done at GSFC (Greenbelt, MD) in the Precipitation Processing System (PPS). JAXA data
193 processing is carried out at the Tsukuba Space Center (Tsukuba, Ibaraki, Japan) in the Mission
194 Operations System (MOS). The interconnected architecture of this joint mission ground system
195 can be seen in Figure 4. Working with the GPM principal investigators and science algorithm
196 developers, PPS maintains the operational science data processing system and ensures the timely
197 processing of all GPM science instrument data [see Hou et al. 2014 for a table of GPM products].
198 During routine operations, raw instrument data (Level 0 data) is received in near-real-time by the
199 PPS and processed using science algorithms to produce calibrated, swath-level instrument (Level
200 1, L1) data. JAXA's MOC processes DPR Level 1 products and their Level 3 merged satellite
201 products. Additional algorithms are used to compute geophysical parameters such as precipitation
202 rate at the swath-level resolution (Level 2, L2 data products). [For reference, a special collection
203 of papers describing the L2 precipitation algorithms is appearing in the *Journal of Atmospheric
204 and Oceanic Technology*.] At the final stage of processing, Level 3 (L3) algorithms produce
205 gridded and accumulated geophysical parameters including products such as latent heating profiles
206 (e.g., Tao et al. 2016). It is envisioned that Level 4 data products developed through model-
207 assimilated precipitation forecast and analysis will be available in the future.

208 The GPM mission has both near-real-time (NRT) and research-quality production
209 requirements. Both NASA and JAXA contribute key processing efforts to fulfill these latency
210 requirements. The NRT products are produced using forecast or earlier forms of ancillary data.

211 NRT products include GMI TB, and precipitation estimates from GMI (denoted GPROF),
212 DPR, and Combined Radar-Radiometer Algorithm (denoted CORRA) (Kummerow et al. 2015,
213 Seto et al. 2015, Grecu et al. 2016). GMI products are available within an hour of data collection
214 while DPR and CORRA are available within 3 hours of data collection. Another NRT product
215 developed by the U.S. team is the Integrated Multi-satellitE Retrievals for GPM (IMERG) gridded
216 retrieval that is a Level 3 NASA product (Huffman et al. 2015). JAXA produces an analogous
217 product called Global Satellite Mapping of Precipitation (GSMaP) (Kubota et al. 2007, Aonashi
218 et al. 2009, Ushio et al. 2009). IMERG uses the GPM-CO to inter-calibrate precipitation data from
219 all constellation radiometers. Temporal and spatial gaps in the IMERG microwave precipitation
220 estimates (e.g., as shown in Figure 3) are filled by morphing the estimates in between the microwave
221 overpasses, and incorporating IR estimates with a Kalman filter where the gaps are too long (over
222 about 3 hours) to produce $0.1^\circ \times 0.1^\circ$ half-hour global products. The IMERG product is produced
223 twice in NRT; once approximately 5 hours after data collection and again approximately 14 hours
224 after data collection.

225 All of the NRT products are also processed as research products. The geolocation of the
226 research products is more consistent as predictive ephemeris rarely needs to be used. Research
227 products are produced by PPS when all the required high quality ancillary and geolocation data
228 are received with the objective for accuracy, completeness, and consistency. These research
229 products are available hours to months after data collection and are stable for long-term

230 precipitation investigations. PPS generates and distributes all data from the instruments on the core
231 satellite as well as Level 2 and Level 3 data from the partner constellation satellites. In addition to
232 the standard HDF5 format files, a Geographic Information System (GIS; TIFF world files) product
233 and ASCII text files are provided for selected product estimates. All GPM data are openly available
234 and accessible from <https://pmm.nasa.gov/data-access/downloads/gpm>. JAXA's GPM products in
235 general can be obtained from <https://www.gportal.jaxa.jp/gp/top.html> while the GSMaP multi-
236 satellite merged data can be obtained from <http://sharaku.eorc.jaxa.jp/>. GPM data (Level 0-3) are
237 periodically reprocessed as retrieval algorithms are improved. The at-launch Version 03 IMERG
238 accumulation products are known to be high biased during heavy rain events and the next IMERG
239 reprocessing to Version 04 (early 2017) is expected to address these high biases. GPM retrieval
240 algorithms use the dual frequency channels of DPR and the high frequency channels of GMI and
241 hence precipitation products from GPM are different than those from TRMM. Nevertheless, there
242 are plans to reprocess inter-calibrated precipitation data (in winter 2017-2018) to produce a
243 consistent long-term precipitation record that starts at the beginning of TRMM. GPM is meeting
244 data latency requirements (as shown in the sidebar), on average, greater than 99% of the time.
245 Recent PPS statistics show nearly 50 TB data downloaded by more than 1,000 unique users from
246 all over the world in a single month.

247

248 **Validation Efforts**

249 GPM Ground Validation (GV) efforts include the direct statistical validation and verification of
250 satellite estimates against high-quality ground measurements, and physical validation for
251 algorithm improvement and hydrological models. Validating data is from both regular ongoing
252 surface observations and focused field campaigns (Hou et al., 2014; see also

253 <https://pmm.nasa.gov/index.php?q=science/ground-validation>). Major GPM validation efforts are:
254 (1) Comparisons among satellite precipitation products, (2) comparisons against ground datasets,
255 and (3) analysis for meeting mission requirements.

256 One evaluation technique compares zonal means among the various GPM instrument
257 algorithms and established precipitation estimates such as the Global Precipitation Climatology
258 Project (GPCP) data sets (Adler et al. 2003) and, over ocean, the Merged CloudSat, TRMM, Aqua
259 version 2 (MCTA2) data (Behrangi et al. 2014). Both GPCP and MCTA2 include a variety of input
260 data sets selected for utility in precipitation estimation at both low and high latitudes. Figure 5 shows
261 the global zonal means for 2015 for land and ocean (Figure 5a), ocean only (Figure 5b), and land only
262 (Figure 5c). This figure illustrates that DPR, Ku, CORRA, and GPROF algorithm retrievals are in
263 good agreement. The GPM zonal accumulations underestimate with respect to the MCTA at higher
264 latitudes. This is most attributable to the fact that the DPR minimum detectable reflectivities
265 correspond to minimum rain rates of approximately 0.2 mm h^{-1} . Since much of the higher latitude
266 precipitation is light, and CORRA and GPROF are based on DPR estimates, GPM is low in the
267 higher latitudes. A high latitude, light precipitation solution for GPROF is being implemented in
268 the upcoming algorithm Version 05 release. The mean daily precipitation in mm day^{-1} for each of
269 the algorithms is provided in Table 2. This table shows that IMERG annual precipitation is lower
270 than the other algorithms while there are interesting differences among the diverse approaches
271 over land. Land surfaces tend to complicate the retrieval process and the various algorithms use
272 different approaches to mitigate surface (emissivity and clutter) issues.

273 Direct statistical GV of GPM rainfall rate estimates relies primarily on existing high-
274 resolution, quality-controlled U.S. national radar network rain rate products such as the NOAA

275 National Severe Storms Laboratory/University of Oklahoma Multi-Radar/Multi-Sensor (MRMS)
276 products (e.g., Zhang et al., 2016 and references therein). Currently, the MRMS system
277 (<http://mrms.ou.edu>) incorporates data from all polarimetric WSR-88D radars (NEXRAD), a large
278 number of automated rain gauge networks, and model analyses in the Continental U.S. (CONUS)
279 and southern Canada. The system creates a gridded mosaic of quantitative precipitation estimates
280 (QPE) products on a $0.01^\circ \times 0.01^\circ$ grid at a 2-minute temporal resolution (Zhang et al. 2016 for
281 most recent updates). Of particular value to GPM GV are MRMS radar-based gauge-adjusted QPE.
282 Collectively, these MRMS products provide an independent and consistent reference for directly
283 evaluating post-launch GPM precipitation products across a large number of meteorological
284 regimes as a function of resolution, accuracy, and sample size (Kirstetter et al. 2012).

285 For continental scale verification of GPM products over CONUS all MRMS data coincident
286 with GPM orbits are continuously processed and saved as a GPM GV dataset ([http://wallops-
287 prf.gsfc.nasa.gov/NMQ/index.html](http://wallops-prf.gsfc.nasa.gov/NMQ/index.html)). In addition to standard MRMS quality control procedures
288 (see Zhang et al. 2016), additional procedures to minimize radar uncertainties are employed to
289 derive a high-quality precipitation reference at the satellite product pixel resolution (Kirstetter et
290 al. 2012). Filtering out instances when the radar-gauge ratios are outside of the range 0.1-10.0
291 further refines the instantaneous gauge bias-corrected MRMS product. In addition only radar data
292 with the best measurement conditions (i.e., no beam blockage and radar beam below the melting
293 layer) defined by a Radar Quality Index (RQI) are retained. Gridded 0.01° MRMS products can
294 then be matched to allow direct comparisons between the surface radar and satellite precipitation
295 products (see Figure 6).

296 Independent comparisons of this GPM GV-MRMS reference data set with two dense, well-
297 maintained, and data quality-controlled NASA rain gauge networks show that for c. 5 km footprint,
298 30 minute accumulations $> 0.5 \text{ mm h}^{-1}$, biases are $< 10\%$ while normalized mean absolute errors
299 (NMAE) are $< 35\text{-}40\%$. These results are consistent with a quantitative assessment of the MRMS
300 accuracy performed at its native resolution (Kirstetter et al. 2015b). Individual satellite radar
301 matches are subsequently averaged to coarser 50 km grids, useful for quick look comparison
302 products (cf. <http://wallops-prf.gsfc.nasa.gov/NMQ/index.html>) and for verifying GPM Level-1
303 science requirements (e.g., Figure 7). Here the increased spatial averaging of the footprints together
304 with removal of outliers (5th and 95th percentile) maintains low-bias while further reducing random
305 error in the MRMS data relative to the 5 km footprint scale mentioned above.

306 The GPM-GV MRMS reference dataset and its derivatives have revealed and quantified
307 several aspects of satellite-estimated rainfall retrieval errors and uncertainties including
308 comparisons of rainfall detectability and rainfall rate distributions (Kirstetter et al. 2014),
309 separation of systematic biases and random errors (Kirstetter et al. 2012), regional precipitation
310 biases (Chen et al. 2013), influence of precipitation sub-pixel variability and surface (Kirstetter et
311 al. 2015b; Carr et al. 2015), and comparison between satellite products (Kirstetter et al. 2013, 2014;
312 Tan et al., 2016a, b).

313 Figure 6 provides an example of comparisons to GPM Core satellite products for
314 instantaneous sampling times (e.g., coincident swath and MRMS sample time) as a density-scatter
315 plot for individual near surface DPR sensor footprint scales (effective resolution 5 km). Here it is
316 important to note that the scatter of the data exhibited in Figure 6 is expected based on the
317 instantaneous nature of the comparison at high spatial resolution (e.g., effective FOV), and the

318 related intrinsic random error associated with matching associated precipitation estimates in time
319 and space between MRMS and GPM L2 data swaths. Comparisons at this scale are best interpreted
320 as a tool for evaluating the broader systematic bias behavior between GPM products using the GV
321 as a third reference.

322 In Figure 6 good agreement between the GV MRMS reference and the near surface DPR-
323 Normal Scan (NS) algorithm Version 04 is evident with a bias (defined as the mean relative error;
324 MRE) and normalized mean absolute error (NMAE) of only -9.8% and 51.7%, respectively. The
325 Normal Scan mode of DPR consists of retrievals using the Ku-band 245 km wide swath data. The
326 agreement is particularly good for rainrates in the 1.0 – 10.0 mm h⁻¹ range. Note that the minimum
327 detectable signal of the DPR (~0.2 mm h⁻¹, in terms of rainfall) and partial beam filling are
328 responsible for scatterplot differences at very low rain rates. Contingency statistics for DPR NS
329 rain detection reveal that for ground “reference” rain rates > 0.2 mm h⁻¹ (the lower requirement
330 threshold specified for DPR rain detection based on radar sensitivity), yield a DPR Probability of
331 Detection (POD) of 64%, False Alarm Rate of 9%, and Heidke Skill Score (HSS) of 37%.

332 GPM Mission Science Requirements (see sidebar) stipulate thresholds for detection, bias,
333 and random error (Hou et al., 2013). For example, rain rate estimates should exhibit a bias and
334 random error of ≤ 50% (25%) at rain rates of 1 mm h⁻¹ (10 mm h⁻¹) for areas of 50 km x 50 km.
335 Figure 7 is presented for the DPR Normal Scan (NS) product as a preliminary example of assessing
336 bias and random error. For non-zero raining pixels in Figure 7, the bias in each reference rain bin is
337 computed as the MRE in percent while for the random error the NMAE is computed with the
338 systematic error (bias) removed. Figure 7 suggests that the above GPM Mission Science
339 Requirements have been met for the DPR example shown and the method used. While these results

340 are encouraging, work is ongoing to further test and refine methodologies for determining product-
341 consistent lower rain rate thresholds for comparing GPM GPROF, CORRA, DPR, and MRMS
342 datasets and for defining error types and to meet the other GPM Mission Science Requirements.

343

344 **Initial Scientific Investigations and Applications**

345 With two years worth of calibrated and validated precipitation estimates, GPM's data are
346 being used for scientific studies (e.g., Liu and Liu 2016, Wentz and Meissner 2016, Panegrossi et
347 al. 2016, and Prakash et al. 2016). Most of the science results are from investigations by members
348 of the NASA Precipitation Measurement Missions science team (in 2016 consisting of 60 Principal
349 Investigators from NASA centers and U.S. universities funded by NASA Headquarters while the
350 Japanese PMM Science Team consists of 41 Principal Investigators). NOAA has a team of 16
351 investigators involved with GPM and more than 20 international no-cost teams also play important
352 roles in GPM science and validation efforts. Herein, two scientific investigations are reported:
353 falling snow retrievals and monsoon studies.

354 Scientifically, retrievals of falling snow from space represent an important data set for
355 understanding the Earth's atmospheric, hydrological, and energy cycles. While satellite-based
356 remote sensing provides global coverage of falling snow events, the science is relatively new and
357 retrievals are still undergoing development addressing challenges such as those listed in
358 Skofronick-Jackson et al. (2015). GPM's mission goal of estimating falling snow is demonstrated
359 in an example from March 17, 2014, just 18 days after launch (Figure 1c). More generally, the GMI
360 observed the average snow rate, maximum snow rate, and fraction of precipitation that fell as snow
361 over the winter of 2014-2015 (Figure 8). While these snow estimates are not fully validated they do
362 support the requirement that GPM detect falling snow. The high rates over the south-central states

363 may not be representative of typical winter conditions, but may have resulted from the occurrence
364 of several heavy snow events in mid-late February of 2015 when GMI had good overpasses. Of
365 particular note for this period were the large snowfall rates along the west coast of Canada and
366 southern coast of Alaska, where coastal topography may enhance local snowfall rates.

367 Looking elsewhere, the GPM mission can track the advance and retreat of India's annual
368 monsoon and the tropical storms that impact India's populations. As shown in Figure 9, GPM
369 observes the detailed structure of the copious monsoon precipitation as it marches from south to
370 north across India over the seasons, with Tropical Cyclone Hudhud (Oct 2014) on the left and
371 Storm Roamu (May 2016) on the far right of the timeline. Figure 9 shows the advance of the
372 monsoon season from offshore in May to inland by July, and the retreat back to the Bay of Bengal
373 from September to November over two years of GPM data. Over longer precipitation records,
374 interannual variations due to the effect of large-scale oceanic or atmospheric patterns or to climate
375 change may be identified, information that is crucial for societal applications and benefit.

376 Integrating satellite observations into land surface modeling systems is a critical
377 component of how to resolve the state of the water cycle and stresses on the system during extreme
378 events. The NASA Land Information System (LIS; Kumar et al. 2006, Peters-Lidard et al. 2007)
379 runs operationally at the Short-term Prediction Research and Transition (SPoRT, 2016) Center
380 (Jedlovec 2013, Zavodsky et al. 2013, Case et al. 2016) at NASA's Marshall Space Flight Center
381 (Xia et al. 2012, Zhang et al. 2016, Vargas et al. 2015) to produce analyses and short term forecasts
382 of soil moisture and other fields. LIS is a land surface modeling and data assimilation framework
383 designed to integrate satellite observations, including GPM and the Soil Moisture Active Passive
384 (SMAP) satellite data (Entekhabi et al., 2010) into the modeling infrastructure

385 (<http://lis.gsfc.nasa.gov/>). The integration of GPM data within LIS, run operationally at SPoRT,
386 can capture soil moisture changes. For example, LIS identified an extreme soil moisture increase
387 the first week of October 2015 when a closed upper low over the Southeastern U.S. combined with
388 a deep tropical moisture plume associated with Hurricane Joaquin, led to historic rainfall over the
389 Carolinas. The SPoRT Center provided model outputs from LIS to Eastern Region NWS forecast
390 offices in near-real-time. In other cases, these data are also used by a variety of end users
391 experimentally for assessing drought, flooding potential, and situational awareness for wildfire
392 and blowing dust. There is great potential in the future for using GPM estimates together with
393 other space-based soil-moisture measurements from SMAP to improve weather and hydrological
394 prediction.

395 The GPM suite of products contributes to a wide range of societal applications such as:
396 tropical cyclone location and intensity, famine early warning, drought monitoring, water resource
397 management, agriculture, numerical weather prediction, land system modeling, global climate
398 modeling, disease tracking, economic studies, and animal migration; many of which were initially
399 developed with TRMM data. Many of these applications require near-real-time data as well as
400 longer-term, well-calibrated precipitation information. IMERG is starting to be used as an input
401 for forecasts in other regions of the world, especially areas lacking adequate ground-based
402 coverage. Selected applications are reported in Kirschbaum et al. (2016), Ward et al. (2015),
403 Kucera et al. (2013), and Kirschbaum and Patel (2016).

404

405 **Conclusions and Next Steps**

406 The Global Precipitation Measurement mission provides unprecedented and highly useful
407 global precipitation datasets. GPM's Core Observatory data are used to inter-calibrate a set of
408 precipitation observations from constellation partner sensors. By merging GPM multi-satellite
409 estimates with other IR satellite data, products with temporal resolutions down to 30 minutes and
410 spatial resolutions as small as 0.1° by 0.1° are possible. Latencies, at 1-5 hours (depending on the
411 product) after data collection, are vital for GPM's operational users. Research quality products
412 (with accuracy requirements as indicated in the Sidebar GPM's Mission Science Requirements)
413 are available later (12 hrs to several months) for intensive scientific studies ranging from
414 diagnosing microphysical precipitation particle characteristics to assessing regional and global
415 patterns of precipitation. The GPM mission provides indispensable precipitation data from micro
416 to local to global scales via retrieved precipitation particle size distributions inside clouds, 5-15
417 km resolution estimates of regional precipitation, and merged global precipitation.

418 GPM's algorithms have been updated several times (currently on Version 04) with an
419 additional update planned for 2017. After the release of Version 05, work will begin to reprocess
420 Level 0-3 products back to the beginning of TRMM (1998) and also for partner satellite data sets
421 to establish a long and consistent record of precipitation. Scientific studies and societal
422 applications using GPM data are ongoing and growing rapidly. Knowing the horizontal and
423 vertical structure of precipitation is important for improving weather forecasting and climate
424 change models. The planned processing of a consistent precipitation record encompassing the
425 TRMM and GPM era will be of high value to future generations of scientific studies and user
426 applications. The consistent TRMM-plus-GPM record will generate interesting scientific insights
427 and re-invigorate applications in hydrological/land surface modeling and numerical weather

428 prediction. Going forward in time, GPM's prime mission lifetime lasts until May 2017 at which
429 time GPM will move into Extended Operations. Current predictions suggest that the station-
430 keeping fuel will last 15 or more years, implying that instruments or spacecraft systems (like the
431 batteries) will likely be the life-limiting factors as long as the fuel requirements do not increase.

432 In quantifying precipitation, a key Earth system component, the GPM mission provides
433 fundamental knowledge of the water cycle and compliments other NASA satellite missions such
434 as the Gravity Recovery and Climate Experiment (GRACE), that measures changes in
435 groundwater levels in underground aquifers (among other observations) (Tapley et al. 2004); the
436 Soil Moisture Active Passive (SMAP) satellite (Entekhabi et al. 2010); Aquarius (while it was
437 operating), that observed ocean salinity (Le Vine et al. 2010); and CloudSat, which measures the
438 properties of clouds and light precipitation (Stephens et al. 2002). Integrated multidisciplinary
439 scientific investigations can provide greater understanding of our complex Earth system. GPM has
440 and will continue to provide valuable and freely accessible precipitation data for science and
441 society.

442

443

444

445 **Acknowledgments**

446 This paper is dedicated to former GPM Project Scientist Arthur Y. Hou (1947-2013). Data are
447 provided by NASA / JAXA. The climatological monsoon dates are from the Indian Meteorology
448 Department. Imagery was generated by NASA Goddard Space Flight Center, including the
449 monsoon visualization by Owen Kelley. PMM Science Team members are acknowledged for their
450 many contributions to GPM science. We thank our three anonymous reviewers for thoughtful and

451 paper-enhancing comments. Funding for this work was provided by NASA Headquarters, NOAA,
452 and JAXA.

453
454

455 **Sidebar 1: GPM’s Mission Science Requirements**

456 Prior to the GPM’s launch in 2014, NASA formally documented Core Observatory requirements
457 to be met within GPM’s 3-year Prime Mission operations period in order for GPM to be deemed
458 fully successful. Several of these requirements dealt with instrument performance or operational
459 elements (e.g., orbit maintained to within ± 1 km of operational orbital attitude) and will not be
460 discussed here. Most of the requirements pertained to scientific accuracy and science data and are
461 key to ensuring stable and validated precipitation products expected by both scientific investigators
462 and application users. Specifically, these science requirements are:

- 463 • Measurements of the same geophysical scenes using both active and passive technique
464 from 65°N to 65°S latitude with mean sampling time of 24 hours
- 465 • Using the DPR:
 - 466 – Quantify rain rates between 0.22 and 110.00 mm h⁻¹
 - 467 – Detect snowfall at an effective resolution of 5 km
- 468 • Using the GMI
 - 469 – Quantify rain rates between 0.2 and 60.0 mm h⁻¹
 - 470 – Detect snowfall at an effective resolution of 15 km
- 471 • Estimate precipitation particle size distribution (e.g., quantitative estimates of precipitation
472 microphysical properties such as the mean median mass diameter of particle size
473 distribution to within ± 0.5 mm.)

- 474 • Provide calibrated ground-based precipitation measurements and associated error
475 characterizations at 50 km horizontal resolution for comparison with space-based radar and
476 radiometer measurements at designated ground validation sites within ground tracks of the
477 GPM Core Observatory.
- 478 – The biases in instantaneous rain rates between the ground-based and space-based
479 estimates should not exceed 50% at 1 mm h⁻¹ or 25% at 10 mm h⁻¹
 - 480 – The random errors between the ground-based and space-based estimates should not
481 exceed 50% at 1 mm h⁻¹ or 25% at 10 mm h⁻¹.
- 482 • In order to provide data in near-real-time for hurricane monitoring, numerical weather
483 prediction, hydrological model forecast and other application and operational uses:
- 484 – Combined radar/radiometer swath products will be available within 3 hours of
485 observation time, 90% of the time, and
 - 486 – Radiometer precipitation products will be available within 1 hour of observation
487 time, 90% of the time.

488 At the time of the writing of this article all science requirements have been shown to have been
489 met but have not been documented in the literature. Several papers are being prepared on proving
490 these requirements and will be included in the AMS Special Collection of GPM Publications.

491

Acronym List

492

493 AMSR2 Advanced Microwave Scanning Radiometer for Earth Observing System 2

494 ASCII American Standard Code for Information Interchange

495 ATMS Advanced Technology Microwave Sounder

496 CNES Centre National d'Etudes Spatiales

497 ISRO Indian Space Research Organisation

498 CONUS Continental US

499 CORRA Combined Radar-Radiometer Algorithm

500 dBZ decibel relative to Z

501 DMSP Defense Meteorological Satellite Program

502 DPR Dual-frequency Precipitation Radar

503 EUMESAT European Union Meteorological Satellites

504 FOV Field of View

505 4D Four-dimensional

506 GCOM-W1 Global Change Observation Mission - Water

507 GCPEX Global Precipitation Measurement Cold Season Precipitation Experiment

508 GIS Geographic Information System

509 GHz Gigahertz

510 GMI GPM Microwave Imager

511 GPCP Global Precipitation Climatology Project

512 GPM Global Precipitation Measurement

513 GPM-CO Global Precipitation Measurement Core Observatory

514	GPROF	Goddard Profiling Algorithm
515	GRACE	Gravity Recovery and Climate Experiment
516	GSFC	Goddard Space Flight Center
517	GSMaP	Global Satellite Mapping of Precipitation
518	GV	Ground Validation
519	HDF5	Hierarchical Data Format
520	IMERG	Integrated Multi-satellitE Retrievals for GPM
521	IR	Infrared
522	JAXA	Japan Aerospace Exploration Agency
523	JPSS1	Joint Polar Satellite System-1
524	JST	Japan Standard Time
525	LIS	Land Information System
526	MAE	Mean Absolute Error
527	MHS	Microwave Humidity Sounder
528	MHz	Megahertz
529	MOS	Mission Operations System
530	MRE	Mean Relative Error
531	MRMS	Multi-Radar/Multi-Sensor
532	MSFC	Marshall Space Flight Center
533	NASA	National Aeronautics and Space Administration
534	NEDT	Noise Equivalent Delta Temperature
535	NEXRAD	Next-Generation Radar

536 NOAA National Oceanic and Atmospheric Administration
537 NPP NASA Postdoctoral Program
538 NRT Near-Real-Time
539 NS Normal Scan
540 NWS National Weather Service
541 PMM Precipitation Measurement Missions
542 PPS Precipitation Processing System
543 QPE Quantitative Precipitation Estimates
544 SAPHIR Sounder for Probing Vertical Profiles of Humidity
545 SMAP Soil Moisture Active Passive
546 SPoRT Short-term Prediction Research and Transition
547 SSMIS Special Sensor Microwave Imager/Sounder
548 TB Brightness Temperature
549 TIFF Tagged Image File Format
550 TMI TRMM Microwave Imager
551 TRMM Tropical Rainfall Measuring Mission
552 3D Three-Dimensional
553 U.S. United States
554 UTC Coordinated Universal Time
555 WMO World Meteorological Organization
556 WSR-88D Weather Surveillance Radar 88 Doppler
557

558

REFERENCES

- 559 Adler, R. F., and Coauthors, 2003: The version-2 global precipitation climatology project
560 (GPCP) monthly precipitation analysis (1979-present). *J. Hydrometeor.*, **4**, 1147-1167.
- 561 Adler, R. F., J. J. Wang, , G. Gu, and G. J. Huffman, 2009: A ten-year tropical rainfall
562 climatology based on a composite of TRMM products. *J. of the Meteor. Soc. of Japan*,
563 **87**, 281-293.
- 564 Aonashi, K., and Coauthors, 2009: GSMaP Passive Microwave Precipitation Retrieval
565 Algorithm: Algorithm Description and Validation. *J. of the Meteor. Soc. of Japan*, **87A**,
566 119-136.
- 567 Behrangi, A., G. Stephens, R. F. Adler, G. J. Huffman, B. Lambriksen, and M. Lebsock, 2014:
568 An Update on the Oceanic Precipitation Rate and Its Zonal Distribution in Light of
569 Advanced Observations from Space. *J. Climate*, **27**, 3957-3965. doi:
570 <http://dx.doi.org/10.1175/JCLI-D-13-00679.1>
- 571 Berg, W., and coauthors, 2016: Intercalibration of the GPM Microwave Radiometer
572 Constellation. *J. Atmos. Oceanic Technol.* doi:10.1175/JTECH-D-16-0100.1, in press.
- 573 Case, J. L., K. D. White, B. Guyer, J. Meyer, J. Srikishen, C. B. Blankenship, and B. T.
574 Zavodsky, 2016: Real-time Land Information System over the Continental U.S. for
575 situational awareness and local numerical weather prediction applications.
576 *30th Conf. Hydrology*, New Orleans, LA, Amer. Meteor. Soc., 3.3. [Available online at
577 <https://ams.confex.com/ams/96Annual/webprogram/Paper287812.html>]
- 578 Carr, N., P. E. Kirstetter, Y. Hong, J. J. Gourley, M. Schwaller, W. Petersen, N.-Y. Wang, R. R.
579 Ferraro, and X. Xue, 2015: The Influence of Surface and Precipitation Characteristics on
580 TRMM Microwave Imager Rainfall Retrieval Uncertainty. *J. Hydrometeor.*, **16**, 1596–
581 1614, doi:10.1175/JHM-D-14-0194.1.
- 582 Chen, S., and Coauthors, 2013: Evaluation of Spatial Errors of Precipitation Rates and Types
583 from TRMM Space-borne Radar over the southern CONUS. *J. Hydrometeor.*, **14**, 1884–
584 1896.
- 585 Curtis, S., A. Salahuddin, R. F. Adler, G. J. Huffman, G. Gu, and Y. Hong, 2007: Precipitation
586 extremes estimated by GPCP and TRMM: ENSO relationships. *J. of Hydrometeor.*, **8**,
587 678-689.
- 588 Draper, D. W., D. A. Newell, D. A. Teusch, and P. K. Yoho, 2013: Global Precipitation
589 Measurement Microwave Imager (GMI) hot load calibration. *IEEE Trans. Geosci. Rem.*
590 *Sens.*, **51**, 4731-4742, doi:10.1109/TGRS.2013.2239300.
- 591 Draper, D. W., D. A. Newell, F. J. Wentz, S. Krimchansky, and G. Skofronick-Jackson, 2015a:
592 The Global Precipitation Measurement (GPM) Microwave Imager (GMI): Instrument
593 Overview and Early On-orbit Performance. *IEEE J. Sel. Topics Geosci. Remote Sens.*, **8**,
594 3452-3462, doi:10.1109/JSTARS.2015.2403303.

595 Draper, D. W., D. A. Newell, D. McKague and J. Piepmeier, 2015b: Assessing Calibration
596 Stability using the Global Precipitation Measurement (GPM) Microwave Imager (GMI)
597 Noise Diodes. *IEEE J. Sel. Topics Geosci. Remote Sens.*, **8**,
598 doi:10.1109/JSTARS.2015.2406661.

599 Entekhabi, D., and Coauthors, 2010: The soil moisture active passive (SMAP) mission.
600 *Proceedings of the IEEE*, **98**, 704-716.

601 Grecu, M., W. S. Olson, S. J. Munchak, S. Ringerud, L. Liao, Z. S. Haddad, B. L. Kelley, and S.
602 F. McLaughlin, 2016: The GPM Combined Algorithm. *J. Atmos. Oceanic Technol.*, **33**,
603 2225-2245.

604 Hou, A. Y., G. Skofronick-Jackson, C. Kummerow, and J. M. Shepherd, 2008: Global
605 Precipitation Measurement, *Chapter 6 in Precipitation: Advances in Measurement,*
606 *Estimation and Prediction*, S. Michaelides, Ed., Springer-Verlag, 540 pp.

607 Hou, A. Y., 2013: NASA GPM Science Implementation Plan,
608 [https://pmm.nasa.gov/sites/default/files/document_files/GPM%20Science%20Implement](https://pmm.nasa.gov/sites/default/files/document_files/GPM%20Science%20Implementation%20Plan%20-%20April%202013.pdf)
609 [ation%20Plan%20-%20April%202013.pdf](https://pmm.nasa.gov/sites/default/files/document_files/GPM%20Science%20Implementation%20Plan%20-%20April%202013.pdf)

610 Hou, A. Y., R. K. Kakar, S. A. Neeck, A. Azarbarzin, C. D. Kummerow, M. Kojima, R. Oki, K.
611 Nakamura, and T. Iguchi, 2014: The Global Precipitation Measurement Mission. *Bull.*
612 *Amer. Meteor. Soc.*, **95**, 701-722, doi:10.1175/BAMS-D-13-00164.1.

613 Houze, R. A., K. L. Rasmussen, M. D. Zuluaga, and S. R. Brodzik, 2015: The variable nature of
614 convection in the tropics and subtropics: A legacy of 16 years of the Tropical Rainfall
615 Measuring Mission satellite. *Reviews of Geophysics*, **53**, 994-1021.

616 Huffman, G. J., D. T. Bolvin, D. Braithwaite, K. Hsu, R. Joyce, P. Xie, 2015: Algorithm
617 Theoretical Basis Document (ATBD) Version 4.5 for the NASA Global Precipitation
618 Measurement (GPM) Integrated Multi-satellitE Retrievals for GPM (I-MERG). *GPM*
619 *Project*, Greenbelt, MD, 30 pp. [Available online at
620 http://pmm.nasa.gov/sites/default/files/document_files/IMERG_ATBD_V4.5.pdf]

621 Jedlovec, G., 2013: Transitioning Research Satellite Data to the Operational Weather
622 Community: The SPoRT Paradigm. *Geoscience and Remote Sensing Newsletter*, March,
623 L. Bruzzone, Ed., Institute of Electrical and Electronics Engineers, Inc., New York, 62-
624 66.

625 Kidd, C., A. Becker, G. J. Huffman, C. L. Muller, P. Joe, G. Skofronick-Jackson, D. B.
626 Kirschbaum, 2016: So, How Much of the Earth's Surface Is Covered by Rain Gauges?
627 *Bull. Amer. Meteor. Soc.*, **97**, in early release. doi:10.1175/BAMS-D-14-00283.1.

628 Kirschbaum, D. B., and Coauthors, 2016: NASA's Remotely-sensed Precipitation: A Reservoir
629 for Applications Users, *Bull. Amer. Meteor. Soc.*, submitted.

630 Kirschbaum, D. B., and K. Patel, 2016: Precipitation data key to food security and public health.
631 *Eos* [https://eos.org/meeting-reports/precipitation-data-key-to-food-security-and-public-](https://eos.org/meeting-reports/precipitation-data-key-to-food-security-and-public-health)
632 [health](https://eos.org/meeting-reports/precipitation-data-key-to-food-security-and-public-health).

633 Kirstetter, P. E., Y. Hong, J. J. Gourley, Q. Cao, M. Schwaller, and W. Petersen, 2014: A
634 research framework to bridge from the Global Precipitation Measurement mission core
635 satellite to the constellation sensors using ground radar-based National Mosaic QPE. In
636 L. Venkataraman, Remote Sensing of the Terrestrial Water Cycle. AGU books
637 Geophysical Monograph Series, Chapman monograph on remote sensing. John Wiley &
638 Sons Inc. ISBN: 1118872037.

639 Kirstetter, P. E., Y. Hong, J. J. Gourley, S. Chen, Z. Flamig, J. Zhang, M. Schwaller, W.
640 Petersen, and E. Amitai, 2012: Toward a Framework for Systematic Error Modeling of
641 Spaceborne Precipitation Radar with NOAA/NSSL Ground Radar-based National Mosaic
642 QPE. *J. of Hydrometeor.*, **13**, 1285-1300.

643 Kirstetter, P. E., Y. Hong, J. J. Gourley, M. Schwaller, W. Petersen, and Q. Cao, 2015a: Impact
644 of sub-pixel rainfall variability on spaceborne precipitation estimation: evaluating the
645 TRMM 2A25 product. *Quart. J. of the Roy. Meteor. Soc.*, **141**, 953–966.

646 Kirstetter, P.E., J.J. Gourley, Y. Hong, J. Zhang, S. Moazamigoodarzi, C. Langston, A. Arthur,
647 2015b: Probabilistic Precipitation Rate Estimates with Ground-based Radar Networks.
648 *Water Resources Research*, 51, 1422–1442. doi:10.1002/2014WR015672

649 Kojima, M., and Coauthors, 2012: Dual-frequency precipitation radar (DPR) development on the
650 global precipitation measurement (GPM) core observatory. Earth Observing Missions
651 and Sensors: Development, Implementation, and Characterization II, H. Shimoda et al.,
652 Eds., International Society for Optical Engineering (SPIE Proceedings, Vol. 8528),
653 85281A, doi: 10.1117/12.976823.

654 Kozi, T., and Coauthors, 2001: Development of Precipitation Radar onboard the Tropical
655 Rainfall Measuring Mission satellite. *IEEE Geosci. Remote Sens. Lett.*, **39**, 102–116.

656 Kubota, T., and Coauthors, 2007: Global Precipitation Map using Satelliteborne Microwave
657 Radiometers by the GSMaP Project: Production and Validation, *IEEE Trans. Geosci.*
658 *Remote Sens.*, Vol. 45, No. 7, pp.2259-2275.

659 Kubota, T., and Coauthors, 2014: Evaluation of precipitation estimates by at-launch codes of
660 GPM/DPR algorithms using synthetic data from TRMM/PR observations,” *IEEE J. Sel.*
661 *Topics Appl. Earth Observ. Remote Sens.*, vol.7, no.9, pp. 3931-3944.
662 doi:10.1109/JSTARS.2014.2320960

663 Kubota, T., T. Iguchi, M. Kojima, L. Liao, T. Masaki, H. Hanado, R. Meneghini, and R. Oki,
664 2016: A statistical method for reducing sidelobe clutter for the Ku-band precipitation
665 radar onboard the GPM Core Observatory. *J. Atmos. Oceanic Technol.*, 33 (7), 1413-
666 1428.

667 Kucera, P. A., E. E. Ebert, F. J. Turk, V. Levizzani, D. Kirschbaum, F. J. Tapiador, A. Loew, and
668 M. Borsche, 2013: Precipitation from space: Advancing Earth system science. *Bull.*
669 *Amer. Meteor. Soc.*, **94**, 365-375.

670 Kumar, S. V, and Coauthors, 2006: Land Information System - An Interoperable Framework for
671 High Resolution Land Surface Modeling. *Environ. Model. Softw.*, **21**, 1402–1415.

672 Kummerow, C. D., D. L. Randel, M. Kulie, N.-Yu Wang, R. Ferraro, S. J. Munchak, and V.
673 Petkovic, 2015: The Evolution of the Goddard PROFiling Algorithm to a Fully
674 Parametric Scheme. *J. Atmos. Oceanic Technol.*, **32**, 2265–2280.

675 Kummerow, C., W. Barnes, T. Kozu, J. Shiue, and J. Simpson, 1998: The Tropical Rainfall
676 Measuring Mission (TRMM) Sensor Package, *J. Atmos. Oceanic Technol.*, **15**, 809–817.

677 Kummerow, C., and Coauthors, 2000: The status of the Tropical Rainfall Measuring Mission
678 (TRMM) after two years in orbit, *J. Appl. Meteor.*, **39**, Part 1, 1965-1982.

679 Kummerow, C. D., S. Ringerud, J. Crook, D. Randel, and W. Berg, 2010: An observationally
680 generated *A-Priori* database for microwave rainfall retrievals, *J. Atmos. Oceanic Tech.*,
681 **28**, 113-130, doi:10.1175/2010JTECHA1468.1.

682 Le Vine, D. M., G. S. E. Lagerloef, and S. E. Torrusio. 2010: Aquarius and remote sensing of sea
683 surface salinity from space. *Proceedings of the IEEE*, **98**, 688-703.

684 Liu, N. and C. Liu, 2016: Global distribution of deep convection reaching tropopause in 1 year
685 GPM observations. *J. of Geophys. Res.: Atmos.*, **121**, 3824-3842.

686 Liu, C., D. J. Cecil, E. J., Zipser, K. Kronfeld, and R. Robertson, 2012: Relationships between
687 lightning flash rates and radar reflectivity vertical structures in thunderstorms over the
688 tropics and subtropics. *J. of Geophys. Res.: Atmos.*, **117**, 19 pp.
689 doi:10.1029/2011JD017123.

690 Liu, C. and E. J. Zipser, 2015: The global distribution of largest, deepest, and most intense
691 precipitation systems. *Geophys. Res. Lett.*, **42**, 3591-3595.

692 Prakash, S., Mitra, A. K., D. S. Pai, and A. AghaKouchak, 2016: From TRMM to GPM: How
693 well can heavy rainfall be detected from space?. *Advances in Water Resources*, **88**, 1-7.

694 Panegrossi, G., and Coauthors, 2015: Use of the constellation of PMW radiometers in the GPM
695 ERA for heavy precipitation event monitoring and analysis during fall 2014 in Italy. In
696 *2015 IEEE International Geoscience and Remote Sensing Symposium (IGARSS)*, 5150-
697 5153).

698 Peters-Lidard, C. D., and Coauthors, 2007: High-performance Earth system modeling with
699 NASA/GSFC's Land Information System. *Innovations Syst. Softw. Eng.*, **3**, 157-165.

700 Seto, S., T. Iguchi, T. Shimozuma, and S. Hayashi, 2015: NUBF correction methods for the
701 GPM/DPR level-2 algorithms. In *2015 IEEE International Geoscience and Remote*
702 *Sensing Symposium (IGARSS)*, 2612-2614.

703 Shepherd, M., T. Mote, J. Dowd, M. Roden, P. Knox, S. C. McCutcheon, S. E. Nelson, 2011: An
704 overview of synoptic and mesoscale factors contributing to the disastrous Atlanta flood of
705 2009. *Bull. Amer. Meteor. Soc.*, **92**, 861-870.

706 Simpson, J. R., R. F. Adler, and G. R. North, 1988: A proposed Tropical Rainfall Measuring
707 Mission (TRMM) satellite, *Bull. Amer. Meteor. Soc.*, **69**, 278–295.

708 Skofronick-Jackson, and Coauthors, 2015: Global Precipitation Measurement Cold Season
709 Precipitation Experiment (GCPEX): For Measurement Sake Let it Snow. *Bull. Amer.*
710 *Meteor. Soc.*, **96**, 1719–1741, doi:10.1175/BAMS-D-13-00262.1.

711 SPoRT website, 2016: [Available online at [https://nasasport.wordpress.com/category/land-](https://nasasport.wordpress.com/category/land-information-system-lis/)
712 [information-system-lis/](https://nasasport.wordpress.com/category/land-information-system-lis/) accessed June 28, 2016; or <http://weather.msfc.nasa.gov/sport/>.

713 Stephens, G. L., and Coauthors, 2002: The CloudSat mission and the A-Train: A new dimension
714 of space-based observations of clouds and precipitation. *Bull. Amer. Meteor. Soc.*, **83**,
715 1771-1790.

716 Tapley, B. D., S. Bettadpur, J. C. Ries, P. F. Thompson, and M. M. Watkins, 2004: GRACE
717 measurements of mass variability in the Earth system. *Science*, **305**, 503-505.

718 Tan, B.-Z., W. A. Petersen, and A. Tokay, 2016 (a): A Novel Approach to Identify Sources of
719 Errors in IMERG for GPM Ground Validation. *J. Hydromet.*, in press.

720 Tan, B.-Z., W. A. Petersen, P. Kirstetter, and Y. Tian, 2016(b): Performance of IMERG as a
721 Function of Spatiotemporal Scale. *J. Hydromet.*, in press

722 Tao, W.-K., and Coauthors, 2016: TRMM latent heating retrieval: Applications and comparisons
723 with field campaigns and large-scale analyses, in Multi-scale Convection-Coupled
724 Systems in the Tropics. *Meteor. Monogr.*, No. 56, 34 pp.

725 Toyoshima, K., H. Masunaga, and F.A. Furuzawa, 2015: Early Evaluation of Ku-and Ka-Band
726 Sensitivities for the Global Precipitation Measurement (GPM) Dual-Frequency
727 Precipitation Radar (DPR). *SOLA*, **11**, 14-17, doi:10.2151/sola.2015-004.

728 Ushio, T. and Coauthors, 2009: A Kalman filter approach to the Global Satellite Mapping of
729 Precipitation (GSMaP) from combined passive microwave and infrared radiometric data.
730 *J. Meteor. Soc. Japan*, 87A, 137-151.

731 Vargas, M., Z. Jiang, J. Ju, and I. A. Csiszar, 2015: Real-time daily rolling weekly Green
732 Vegetation Fraction (GVF) derived from the Visible Imaging Radiometer Suite (VIIRS)
733 sensor onboard the SNPP satellite. *20th Conf. Satellite Meteorology and Oceanography*,
734 Phoenix, AZ, Amer. Meteor. Soc., P210. [Available online at
735 <https://ams.confex.com/ams/95Annual/webprogram/Paper259494.html>]

736 Xia, Y., and Coauthors, 2012: Continental-scale water and energy flux analysis and validation
737 for the North American Land Data Assimilation System project phase 2 (NLDAS-2): 1.
738 Intercomparison and application of model products. *J. Geophys. Res.*, **117**, 27 pp.
739 doi:10.1029/2011JD016048.

740 Ward, A., D. Kirschbaum, and M. Hobish, 2015: Measuring Rain and Snow for Science and
741 Society: The Second GPM Applications Workshop. *Earth Obs.*, **27**, 4–11.
742 http://eosps.nasa.gov/sites/default/files/eo_pdfs/Sep_Oct_2015_color_508.pdf#page=4.

743 Wentz, F. J. and D. Draper, 2016: On-Orbit Absolute Calibration of the Global Precipitation
744 Measurement Microwave Imager. *J. Atmos. Oceanic Technol.*, **33**, in early release.
745 doi:10.1175/JTECH-D-15-0212.1.

746 Wentz, F. J., T. Meissner, 2016: Atmospheric Absorption Model for Dry Air and Water Vapor at
747 Microwave Frequencies below 100 GHz Derived from Spaceborne Radiometer
748 Observations. *Radio Science*, **51**, 381-391. doi:10.1002/2015RS005858.

749 Wilheit, T., 2013: Comparing calibrations of similar conically-scanning window-channel
750 microwave radiometers. *IEEE Trans. Geosci. Rem. Sens.*, **51**, 1453-1464.
751 doi:10.1109/TGRS.2012.2207122.

752 Wilheit, T., W. Berg, H. Ebrahimi, R. Kroodsmas, D. McKague, V. Payne, and J. Wang, 2015:
753 Intercalibrating the GPM constellation using the GPM microwave imager (GMI).
754 *Geoscience and Remote Sensing Symposium (IGARSS), 2015 IEEE International*,
755 doi:10.1109/IGARSS.2015.7326996.

756 Zavodsky, B. T., J. L. Case, C. B. Blankenship, W. L. Crosson, and K. D. White, 2013:
757 Application of next-generation satellite data to a high-resolution, real-time land surface
758 model. *Earthzine*, J. Kart, Ed., Institute of Electrical and Electronics Engineers
759 [Available online at [http://www.earthzine.org/2013/04/10/application-of-next-generation-
760 satellite-data-to-a-high-resolution-real-time-land-surface-model/.](http://www.earthzine.org/2013/04/10/application-of-next-generation-satellite-data-to-a-high-resolution-real-time-land-surface-model/)]

761 Zhang J., and Coauthors, 2011: National Mosaic and multi-sensor QPE (NMQ) system:
762 Description, results, and future plans. *Bull. Amer. Meteor. Soc.*, **92**, 1321-1338.

763 Zhang, J., and Coauthors, 2016: Multi-Radar Multi-Sensor (MRMS) Quantitative Precipitation
764 Estimation: Initial Operating Capabilities. *Bull. Amer. Meteor. Soc.*, **97**, 621-638.

765

766 Table 1: Channel availability by frequency and polarization (V=Vertically polarized,
767 H=Horizontally polarized) for the GPM constellation radiometers. GMI, TMI, AMSR2, and
768 SSMIS are all conically scanning imagers while MHS, ATMS, and SAPHIR are cross-track
769 scanning water vapor sounders. ATMS is currently operating on board Suomi NPP with a second
770 copy to launch on board JPSS1 in mid 2017.

Sensor	Satellite	6-7 GHz	10 GHz	18-19 GHz	21-23 GHz	31-37 GHz	85-92 GHz	150-166 GHz	183 GHz
GMI	GPM		10.65 VH	18.7 VH	23.8 V	36.64 VH	89.0 VH	166 VH	183.31 V ± 3 , ± 7
TMI	TRMM		10.65 VH	19.35 VH	21.3 V	37.0 VH	85.5 VH		
AMSR2	GCOM-W1	6.925 VH 7.3 VH	10.65 VH	18.7 VH	23.8 VH	36.5 VH	89.0 VH		
SSMIS	DMSP F16, F17, F18, F19			19.35 VH	22.235 V	37.0 VH	91.655 VH	150 H	183.31 H ± 1 , ± 3 , ± 6.6
MHS	NOAA-18/19, MetOp-A/B						89 V	157 V	183.31 H ± 1 , ± 3 , 190.31V
ATMS	Suomi NPP, JPSS1				23.8 V	31.4 V	88.2 V	165.5 H	183.31 H ± 1 , ± 1.8 , ± 3 , ± 4.5 , ± 7
SAPHIR	Megha- Tropiques								183.31 H ± 0.2 , ± 1.1 , ± 2.8 , ± 4.2 , ± 6.8 , ± 11

771
772
773
774

775 Table 2: Area weighted mean annual precipitation in mm day⁻¹ for each of the algorithms
 776 globally, over land, and over ocean from +/- 50 degrees latitude.

	Global Mean Daily Precipitation	Oceanic Mean Daily Precipitation	Land Mean Daily Precipitation
DPR	2.51	2.77	1.72
GPROF	2.86	2.99	2.36
Ku	2.81	3.03	2.05
CORRA	2.83	2.85	2.77
IMERG	2.48	2.44	2.39
GPCP	2.95	3.15	2.43
GSMaP	2.74	2.83	2.12

777
778

779 Figure 1: GPM-CO GMI composite brightness temperatures and example precipitation event
780 cases. Center panel: composite 89 GHz brightness temperatures averaged over 24 months
781 showing the latitudinal extent of the GPM-CO measurements. Example precipitation cases (a) A
782 North Pacific frontal system from GMI, (b) Severe storms in Texas from GMI, (c) winter storm
783 over the Eastern U.S. as observed in 3D from the DPR, (d) North Atlantic winter storm from
784 GMI, (e) Typhoon Fantala as observed in 3D from the DPR, (f) Typhoons Chan-Hom and
785 Nangka in two successive orbits from GMI, (g) a South Pacific frontal system from GMI, (h) a
786 South Atlantic frontal system from GMI, (i) a line of convection in Africa in 3D from the DPR,
787 (j-k) Sumatra land/sea convection day and night from GMI, and (l) an Australian weather system
788 from GMI.

789 Figure 2: Integrated Multi-satellitE Retrievals for GPM (IMERG) accumulated precipitation
790 totals from 4-11 August 2014. The IMERG retrieval algorithm has not yet been developed for
791 pole-to-pole retrievals. The large accumulation near Japan is Typhoon Halong. The accumulation
792 also shows a major storm over the North Sea near Europe, the origins of Hurricane Gonzalo on
793 the western coast of Africa, and a deep tropical depression that produced floods across northern
794 India. IMERG gridded products are produced every 30 minutes with $0.1^\circ \times 0.1^\circ$ grid boxes,
795 currently covering the latitude band 60°N-S .

796 Figure 3: Precipitation estimates are shown for a single orbit of each of the GPM constellation
797 radiometer types for January 1, 2015. The conically-scanning window-channel radiometers are
798 shown on the left and the cross-track scanning water vapor sounding radiometers are shown on
799 the right. The constellation radiometers include a) TMI and GMI on board the NASA TRMM
800 and GPM satellites, b) ATMS on board NOAA's Suomi NPP satellite, c) AMSR2 on board

801 JAXA's GCOM-W1 satellite, d) SAPHIR on board the CNES-ISRO Megha-Tropiques satellite,
802 e) SSMIS on board the DMSP F16, F17, F18 and F19 satellites, and f) MHS on board the
803 NOAA-18, NOAA-19, and EUMETSAT MetOp-A and Metop-B satellites.

804

805 Figure 4: GPM mission operations data and communication system. GPM-CO satellite data are
806 downlinked in near-real-time via the NASA Tracking and Data Relay Satellite System (TDRSS)
807 to White Sands, New Mexico, where the GPM Mission Operations Center retrieves it, ensures its
808 integrity and passes it to PPS. Partner data, ancillary information and validation measurements
809 are also processed by mission operations.

810

811 Figure 5: Zonal precipitation averages (in mm day^{-1}) for the full annual cycle in 2015. The five
812 estimates are: GPM DPR (dual-frequency radar in red), GPM GPROF (GMI passive radiometer
813 in blue), GPM Ku (single-frequency radar in green), GPM CORRA (DPR+GMI in orange),
814 IMERG (GPM merged with constellation estimates in purple), GPCP global estimates (in light
815 blue), and MCTA2 estimates over ocean (in black, covering the years 2007-2010). The GPCP is
816 Version 2.3, MCTA is Version 2, IMERG is Version 03, and the other GPM products are
817 Version 04.

818

819 Figure 6: Density scatterplot of DPR-Normal Scan V04 versus reference MRMS precipitation
820 (mm h^{-1}) at the footprint scale over the period June 2014 - August 2015. The 1:1 line (solid line)
821 is displayed as well as the detection limit for the DPR (0.22 mm h^{-1}). The data shown focuses on

822 the conditional case of satellite footprint and reference mean precipitation rates both nonzero ($>$
823 0.01 mm h^{-1}), and a precipitation type of liquid only.

824

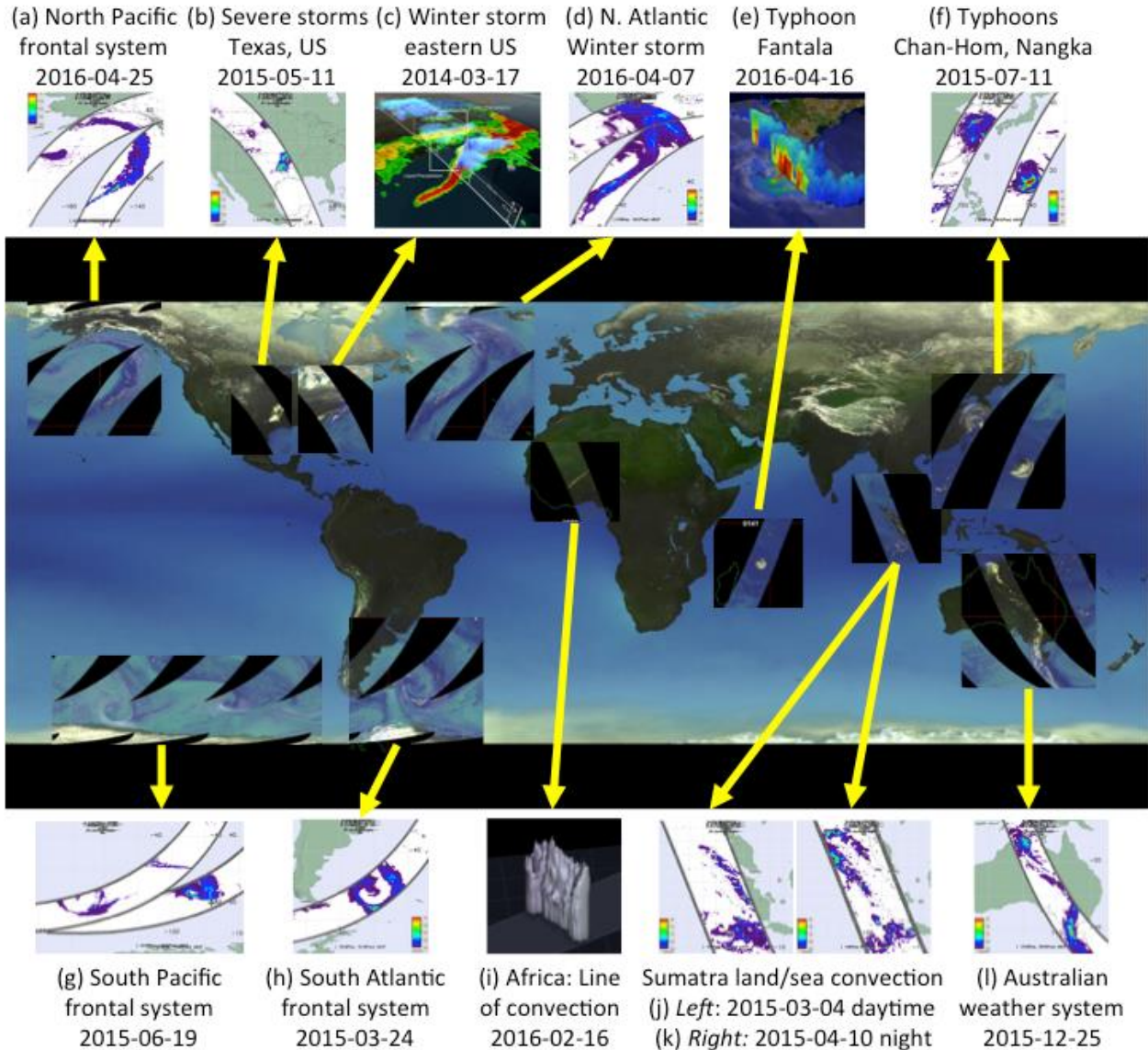
825 Figure 7: Conditional DPR V04 bias (MRE; solid black line) and random error (mean absolute
826 error; dashed black line) versus the MRMS reference precipitation rate (mm h^{-1}) at 50 km
827 resolution over the period June 2014 - August 2015 and normalized by the bin mean rain rate.
828 Points falling outside of the 5%-95% inter-quantile range (outliers) were not included in this
829 comparison. The dashed red lines indicate the GPM Mission Science Requirements 50% (25%)
830 at the specified precipitation rates of 1.0 (10.0) mm h^{-1} .

831

832 Figure 8: The (a) average and (b) maximum liquid equivalent snowfall rates, and (c) fraction of
833 precipitation that was identified as falling snow (and not liquid rain) from December 2014 –
834 February 2015 from the GMI GPROF (Version 04) retrieval algorithm.

835

836 Figure 9: GPM depicts characteristics of India's monsoon seasons in 2014 and 2015. The time-
837 latitude figure (main panel) summarizes the IMERG precipitation estimates over India from
838 April 2014 through May 2016. The heavy, black, dashed line shows the climatological advance
839 and retreat of India's monsoon. The dates of the climatological advance and retreat are shown
840 also on the two maps on the upper left. The area over which IMERG was averaged is indicated
841 by the blue-gray rectangle stretching across India and the Bay of Bengal; the latitude on the main
842 panel is along the mid-line of the rectangle, and the averages are taken along the perpendiculars
843 to the mid-line.



845

846

847

848

849

850

851

852

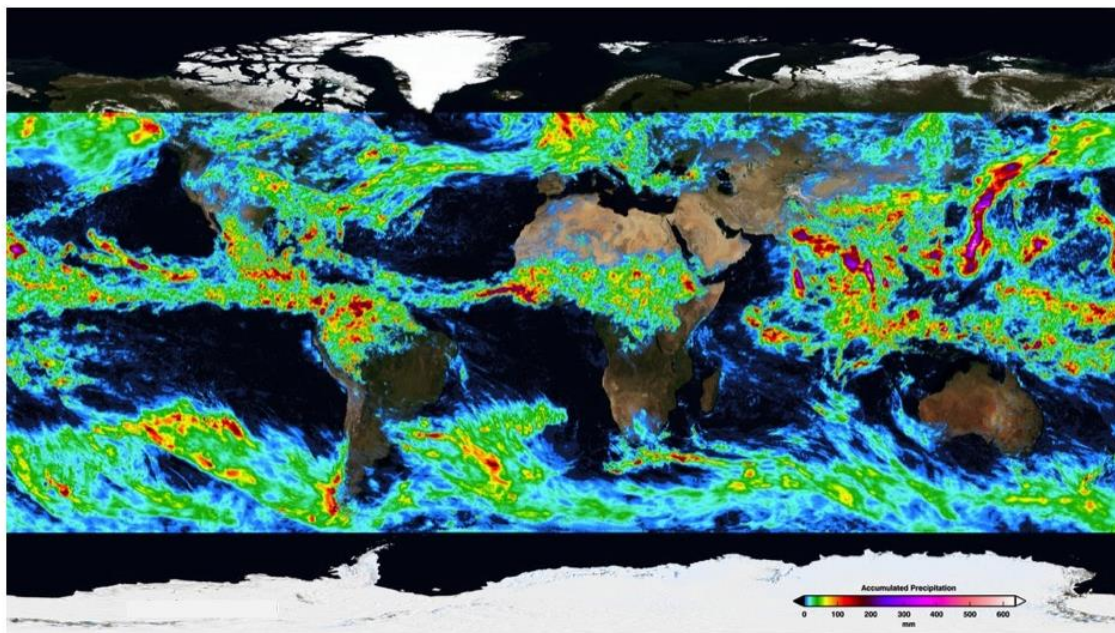
853

854

855

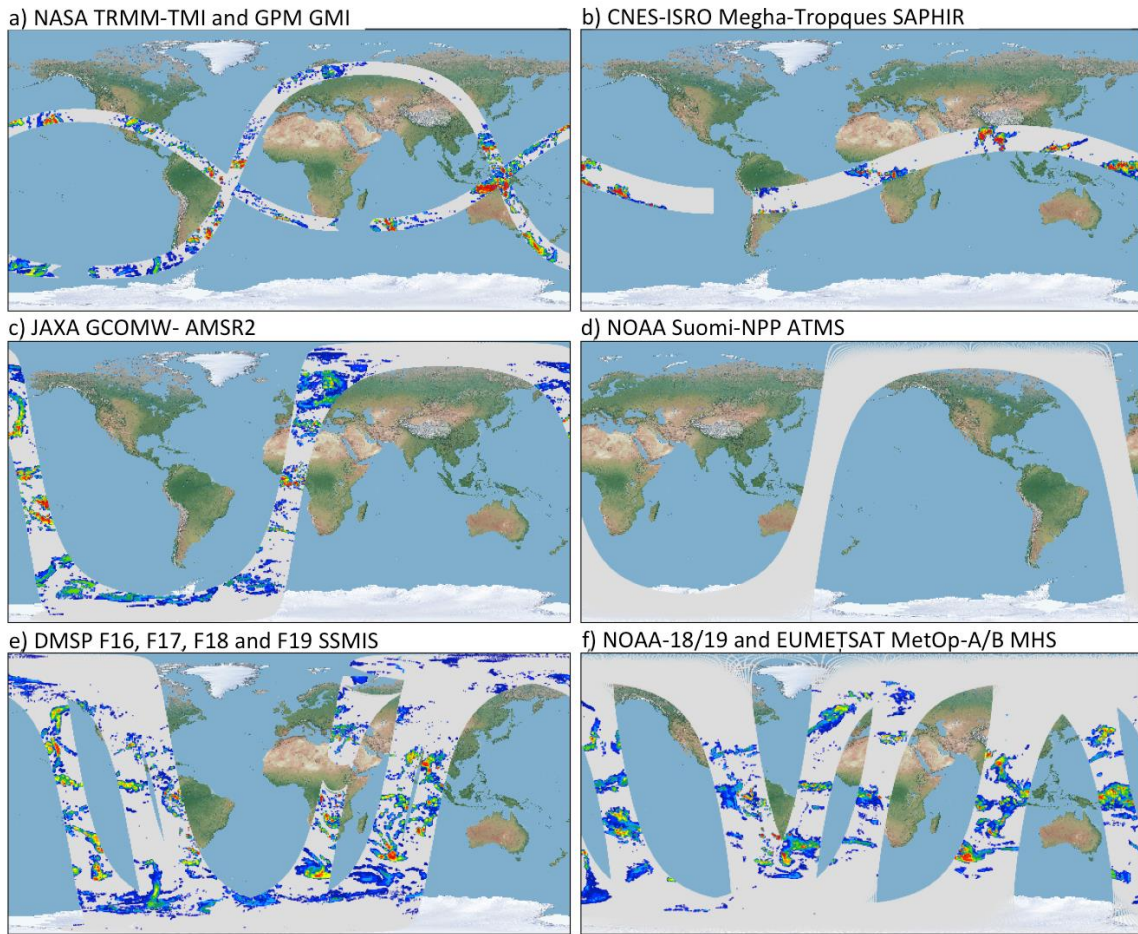
Figure 1: GPM-CO GMI composite brightness temperatures and example precipitation event cases. Center panel: composite 89 GHz brightness temperatures averaged over 24 months showing the latitudinal extent of the GPM-CO measurements. Example precipitation cases (a) A North Pacific frontal system from GMI, (b) Severe storms in Texas from GMI, (c) winter storm over the Eastern U.S. as observed in 3D from the DPR, (d) North Atlantic winter storm from GMI, (e) Typhoon Fantala as observed in 3D from the DPR, (f) Typhoons Chan-Hom and Nangka in two successive orbits from GMI, (g) a South Pacific frontal system from GMI, (h) a South Atlantic frontal system from GMI, (i) a line of convection in Africa in 3D from the DPR, (j-k) Sumatra land/sea convection day and night from GMI, and (l) an Australian weather system from GMI.

856
857
858



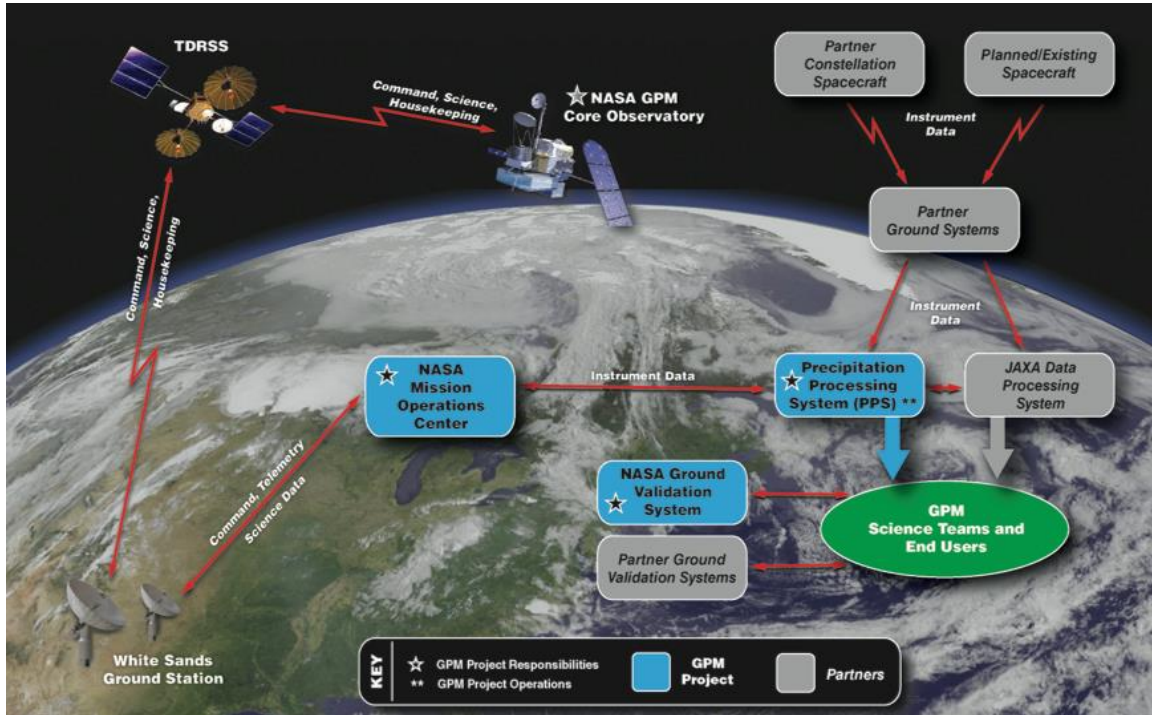
859

860 Figure 2: Integrated Multi-satellite Retrievals for GPM (IMERG) accumulated precipitation
861 totals from 4-11 August 2014. The IMERG retrieval algorithm has not yet been developed for
862 pole-to-pole retrievals. The large accumulation near Japan is Typhoon Halong. The accumulation
863 also shows major storm over the North Sea near Europe, the origins of Hurricane Gonzalo on the
864 western coast of Africa, and a deep tropical depression that produced floods across northern
865 India. IMERG gridded products are produced every 30 minutes with $0.1^\circ \times 0.1^\circ$ grid boxes,
866 currently covering the latitude band 60°N-S .



867
 868
 869
 870
 871
 872
 873
 874
 875
 876
 877

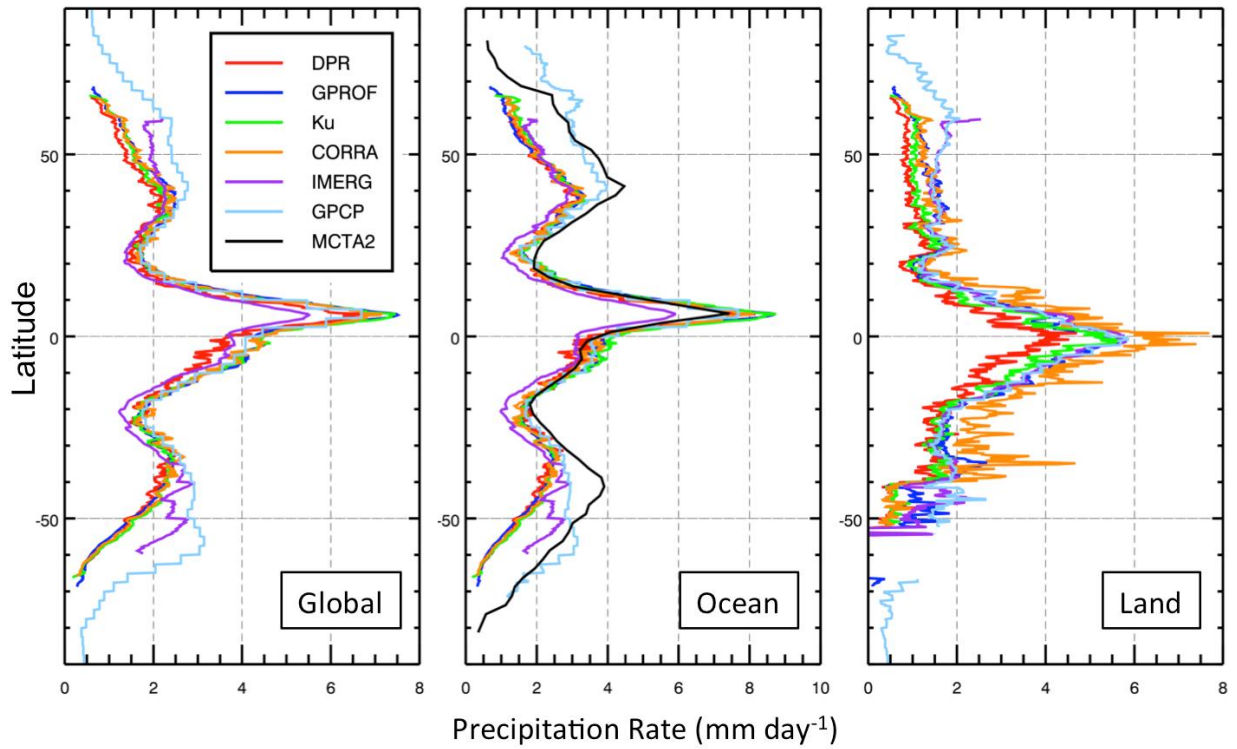
Figure 3: Precipitation estimates are shown for a single orbit of each of the GPM constellation radiometer types for January 1, 2015. The conically-scanning window-channel radiometers are shown on the left and the cross-track scanning water vapor sounding radiometers are shown on the right. The constellation radiometers include a) TMI and GMI on board the NASA TRMM and GPM satellites, b) ATMS on board NOAA’s Suomi NPP satellite, c) AMSR2 on board JAXA’s GCOM-W1 satellite, d) SAPHIR on board the CNES-ISRO Megha-Tropiques satellite, e) SSMIS on board the DMSP F16, F17, F18 and F19 satellites, and f) MHS on board the NOAA-18, NOAA-19, and EUMETSAT MetOp-A and Metop-B satellites.



878
 879
 880
 881
 882
 883
 884
 885
 886
 887

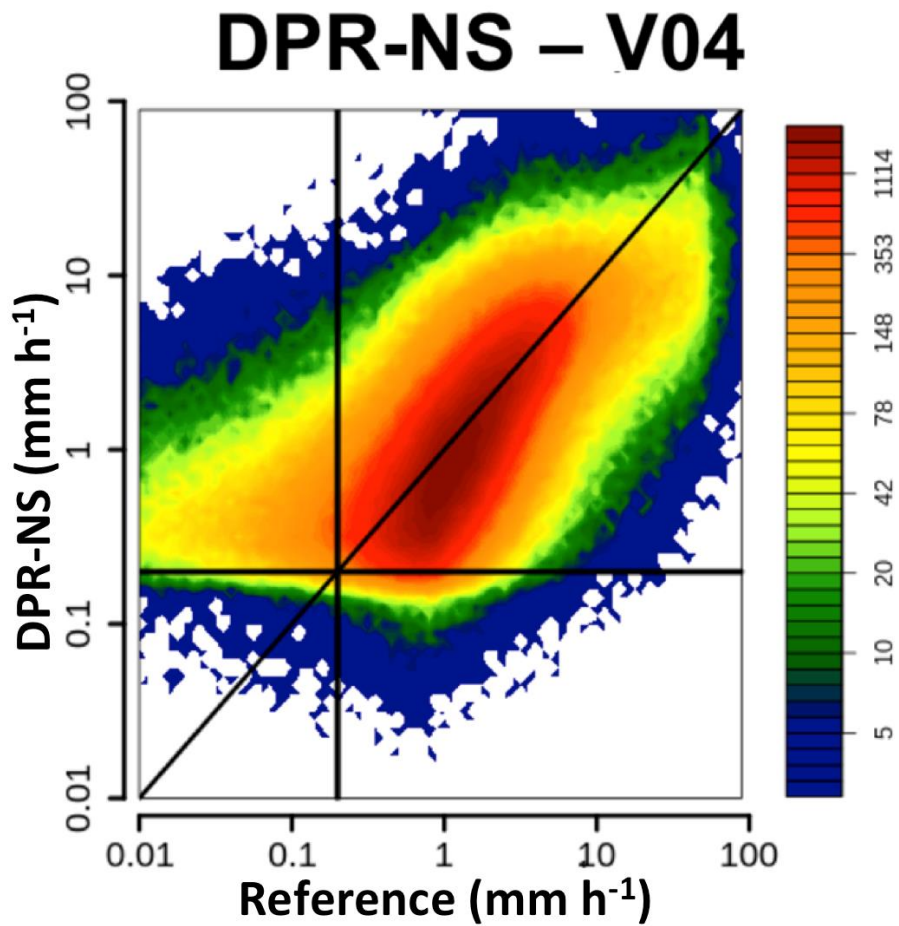
Figure 4: GPM mission operations data and communication system. GPM-CO satellite data are downlinked in near-real-time via the NASA Tracking and Data Relay Satellite System (TDRSS) to White Sands, New Mexico, where the GPM Mission Operations Center retrieves it, ensures its integrity and passes it to PPS. Partner data, ancillary information and validation measurements are also processed by mission operations.

Zonal Mean Annual Accumulations



888
889 Figure 5: Zonal precipitation averages (in mm day^{-1}) for the full annual cycle in 2015. The five
890 estimates are: GPM DPR (dual-frequency radar in red), GPM GPROF (GMI passive radiometer
891 in blue), GPM Ku (single-frequency radar in green), GPM CORRA (DPR+GMI in orange),
892 IMERG (GPM merged with constellation estimates in purple), GPCP global estimates (in light
893 blue), and MCTA2 estimates over ocean (in black, covering the years 2007-2010). The GPCP is
894 Version 2.3, MCTA is Version 2, IMERG is Version 03, and the other GPM products are
895 Version 04.

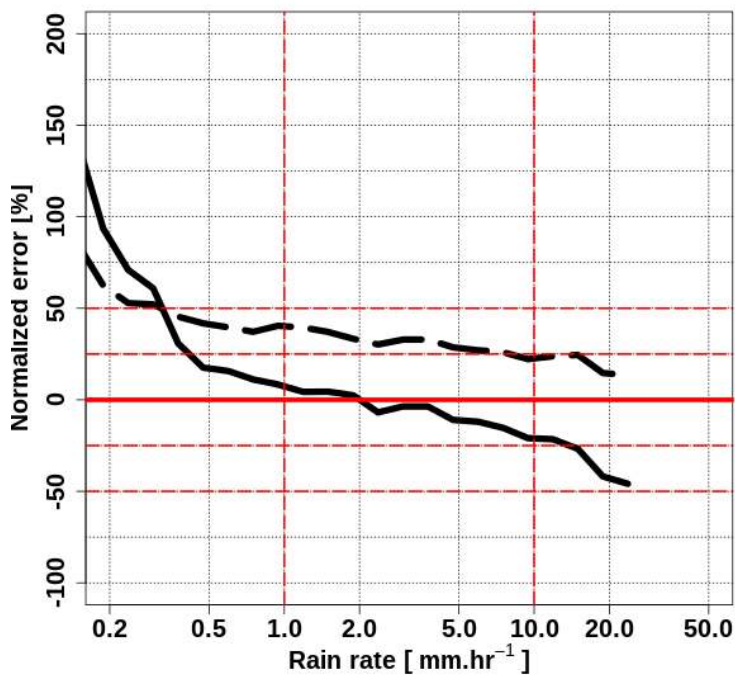
896
897
898
899



900
 901 Figure 6: Density scatterplot of DPR-Normal Scan V04 versus reference MRMS precipitation
 902 (mm h^{-1}) at the footprint scale over the period June 2014 - August 2015. The 1:1 line (solid line)
 903 is displayed as well as the detection limit for the DPR (0.22 mm h^{-1}). The data shown focuses on
 904 the conditional case of satellite footprint and reference mean precipitation rates both nonzero ($>$
 905 0.01 mm h^{-1}), and a precipitation type of liquid only.

906

907



908

909

910

911

912

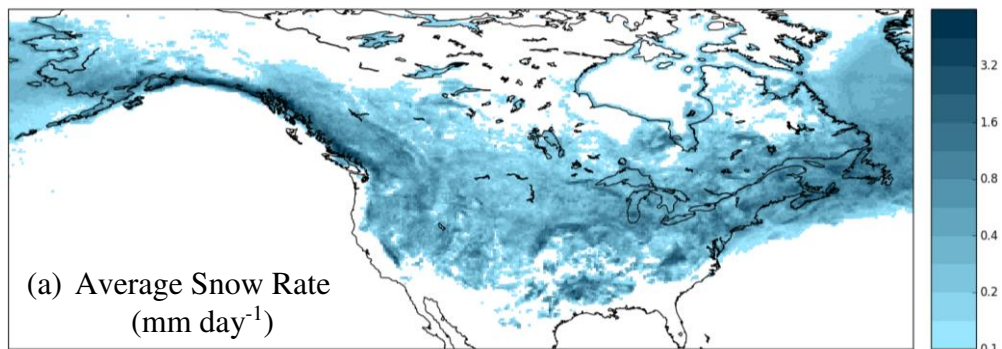
913

914

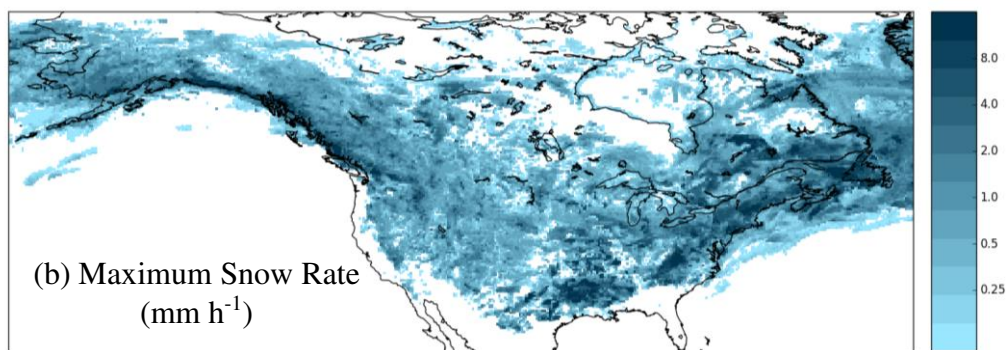
915

Figure 7: Conditional DPR V04 bias (MRE; solid black line) and random error (mean absolute error; dashed black line) versus the MRMS reference precipitation rate (mm h⁻¹) at 50 km resolution over the period June 2014 - August 2015 and normalized by the bin mean rain rate. Points falling outside of the 5%-95% inter-quantile range (outliers) were not included in this comparison. The dashed red lines indicate the GPM Mission Science Requirements 50% (25%) at the specified precipitation rates of 1.0 (10.0) mm h⁻¹.

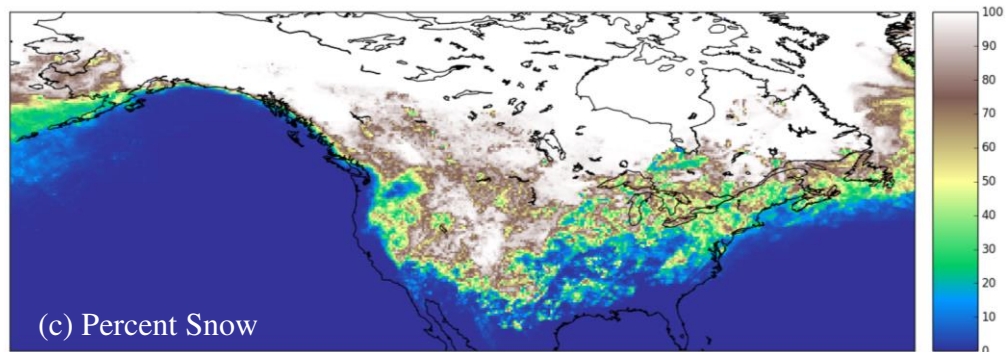
916



917



918



919

920

921

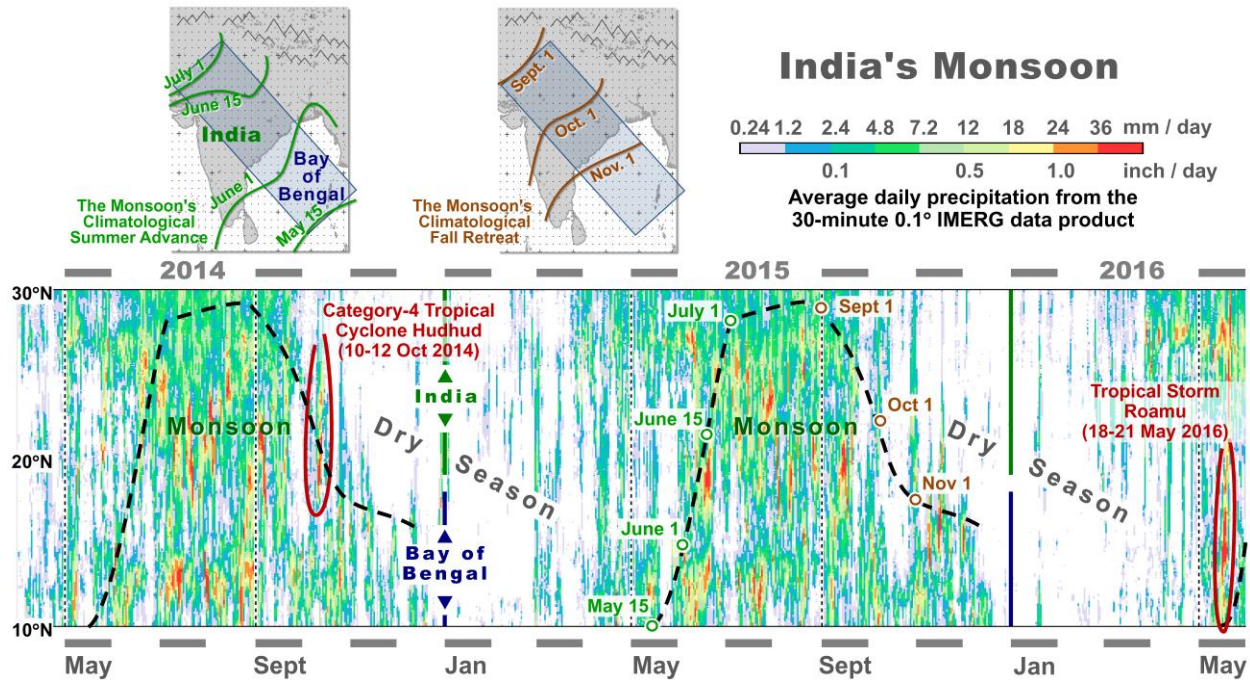
922

923

924

925

Figure 8: The (a) average and (b) maximum liquid equivalent snowfall rates, and (c) fraction of precipitation that was identified as falling snow (and not liquid rain) from December 2014 – February 2015 from the GMI GPROF (Version 04) retrieval algorithm. The average snow rate includes zeros. The maximum is the maximum observed over the whole time period.



926
927
928
929
930
931
932
933
934
935
936

Figure 9: GPM depicts characteristics of India's monsoon seasons in 2014 and 2015. The time-latitude figure (main panel) summarizes the IMERG precipitation estimates over India from April 2014 through May 2016. The heavy, black, dashed line shows the climatological advance and retreat of India's monsoon. The dates of the climatological advance and retreat are shown also on the two maps on the upper left. The area over which IMERG was averaged is indicated by the blue-gray rectangle stretching across India and the Bay of Bengal; the latitude on the main panel is along the mid-line of the rectangle, and the averages are taken along the perpendiculars to the mid-line.